Materials Science and Engineering A 527 (2010) 3602–3608

Contents lists available at ScienceDirect

Materials Science and Engineering A

journal homepage: www.elsevier.com/locate/msea

Annealing behavior of ferritic–martensitic 9%Cr–ODS–Eurofer steel

H.R.Z. Sandim[a,*], R.A. Renzetti[a], A.F. Padilha[b], D. Raabe[c], M. Klimenkov[d], R. Lindau[d], A. Möslang[d]

[a] Department of Materials Engineering, EEL-USP, 12600-970 Lorena, Brazil
[b] Department of Metallurgical and Materials Engineering, Escola Politécnica – USP, 05508-900 São Paulo, Brazil
[c] Max-Planck-Institut für Eisenforschung, D-40237 Düsseldorf, Germany
[d] Karlsruher Institut für Technologie (KIT), IMF I, PO Box 3640, 72061 Karlsruhe, Germany

ARTICLE INFO

Article history:
Received 18 December 2009
Received in revised form 15 February 2010
Accepted 17 February 2010

Keywords:
Steel
Thermomechanical processing
Recrystallization
EBSD

ABSTRACT

Oxide dispersion strengthened ferritic–martensitic steels are potential candidates for applications in future fusion power plants. High creep resistance, good oxidation resistance, reduced neutron activation and microstructural long-term stability at temperatures of about 650–700 °C are required in this context. In order to evaluate its thermal stability in the ferritic phase field, samples of the reduced activation ferritic–martensitic 9%Cr–ODS–Eurofer steel were cold rolled to 50% and 80% reductions and further annealed in vacuum from 300 to 800 °C for 1 h. The characterization in the annealed state was performed by scanning electron microscopy in the backscattered electron mode, high-resolution electron backscatter diffraction and transmission electron microscopy. Results show that the fine dispersion of Y-based particles (about 10 nm in size) is effective to prevent recrystallization. The low recrystallized volume fraction (<0.1) is associated to the nuclei found at prior grain boundaries and around large $M_{23}C_6$ particles. Static recovery was found to be the predominant softening mechanism of this steel in the investigated temperature range.

1. Introduction

Oxide dispersion strengthened materials are good candidates for high-temperature applications including the manufacture of structural parts for nuclear fusion technology. Within the worldwide fusion community, the major objective is the development of structural materials with high irradiation resistance, high mechanical strength and ductility and low activation. The latter means, that their composition should make radioactive activation when exposed to neutron irradiation as low and quickly decaying as possible, thus allowing simple re-use or disposal. As a result, candidate fusion structural materials and plasma facing materials should consist of the following low or reduced activation elements to meet low level waste criteria: Cr, Ti, V, Fe, W, Si, and C [1,2].

Because of the creep properties, RAFM–9%CrWVTa steels [3–5] are presently limited to an upper operating temperature of about 550 °C. The replacement of RAFM steels by suitable ODS alloys would allow a substantial increase of the operating temperature to about 650 °C or even more [6,7]. The addition of nanoscaled ODS particles (Y_2O_3 or $Ti_2Y_2O_7$) is multifunctional: originally to increase high-temperature creep resistance. But meanwhile it has been recognized that – if the trapping strength at the matrix–particle surface is high enough – they could also trap noble gases like helium, or suppress/retard materials aging at high temperature. The matrix–particle interface should act as "market place" for trapping and recombination of irradiation induced defects, trapping of diffusing atoms like Cr, Nb, Mo and V that otherwise might be the origin of alloy dissolution and aging embrittlement.

At the mesoscale, a proper dispersion of fine and chemically stable particles is very effective to interact with mobile dislocations and also with low and high angle boundaries rendering recrystallization very sluggish or even leading to its suppression. This effect is referred to as Zener pinning. The Zener drag is proportional to the grain boundary energy (γ_b), hence the interaction with low angle interfaces is rather small owing to the Read–Shockley relation between interface energy and misorientation angle. On the other hand, individual particles or particle aggregates with sizes above 100 nm tend to speed up recrystallization via the particle stimulated nucleation (PSN) mechanism [8]. Deformed and re-oriented regions around large particles increase the stored energy locally by forming highly misoriented subgrains (nuclei) able to trigger recrystallization and sustain their growth upon subsequent annealing [9]. The kinetics of static recrystallization in particle-containing materials depends on the balance between these driving (stored dislocations) and retarding pressures (Zener drag) in the deformed microstructure. Therefore, the amount of applied strain, particle volume fraction, size distribution and spacing are key parameters to estimate whether a material can undergo recrystallization [10,11].

* Corresponding author at: Department of Materials Engineering, EEL-USP, PO Box 116, 12600-970 Lorena, Brazil. Tel.: +55 12 3159 9916; fax: +55 12 3153 3006.
E-mail address: hsandim@demar.eel.usp.br (H.R.Z. Sandim).

0921-5093/$ – see front matter © 2010 Elsevier B.V. All rights reserved.
doi:10.1016/j.msea.2010.02.051

The material chosen for the present investigation is a 9%Cr–ODS–RAFM–Eurofer steel. It has a microstructure where a fine dispersion of Y-based particles with diameter in the range 10–12 nm coexist with coarse $M_{23}C_6$ (M = Cr, Fe) carbides with sizes of about 0.2–1 μm in the tempered condition [12]. Other minor phases like NbC, VN and the Laves compounds Fe_2Mo and Fe_2W have also been reported in this steel [12]. The $M_{23}C_6$ (M = Cr, Fe) carbide particles are most frequently observed at low and high angle boundaries whereas NbC and VN particles are found in the interior of the ferritic grains after tempering [13]. Pešička et al. reported very inhomogeneous microstructures of this steel in the tempered condition which were characterized by the coexistence of recovered and recrystallized regions [14].

Complex microstructures like that are very interesting model systems for recrystallization studies. The aim of this paper is to study the annealing behavior and the microstructural stability of cold rolled 9%Cr–ODS–Eurofer steel in the ferritic phase field. Electron backscatter diffraction (EBSD) and transmission electron microscopy (TEM) were the main characterization techniques used to follow the microstructural changes in this steel.

2. Experimental

The RAFM–9%Cr–ODS–Eurofer steel has been produced in cooperation with Plansee AG (Austria). The initial RAFM steel powder together with the Y_2O_3 powder was mechanically alloyed. After hot-isostatic pressing, sintered slabs were hot cross-rolled in the austenitic field and then air cooled. The nominal composition of this steel is 9Cr–1W–0.08Ta–0.2V–0.07C–0.4Mn–0.3Y_2O_3 (in wt%). For details, see Ref. [6].

The hot-rolled sheets were tempered at 750 °C for 2 h for the recrystallization study since martensite forms in this steel even when it is air cooled (cooling rate of 5 K/min [4]). The contents of critical elements regarding neutron activation during service life like niobium and cobalt must be kept at very low levels, 0.00021 and 0.0111 wt%, respectively. The carbon and nitrogen contents are, respectively, 0.144 and 0.0278 wt%. Sheets of the ODS–Eurofer steel with dimensions of 80 mm × 200 mm × 6 mm were cold rolled to 50% and 80% thickness reductions in multiple passes. The Vickers microhardness of the steel in the as-received condition was 340 ± 4 HV-0.2. The hardness values after 50% and 80% reductions are, respectively, 391 ± 4 and 425 ± 5 (HV-0.2). Samples were then annealed in vacuum from 300 °C up to 800 °C with a holding time of 1 h. Dilatometric tests were carried out in vacuum (10^{-1} mbar) to determine the A_{c1} and A_{c3} temperatures to set the maximum admissible annealing temperature in the ferritic field using an Adamel Lhomargy dilatometer. This equipment allows heating rates as high as 50 K/s in the samples. The maximum temperature was limited to 1100 °C for a holding time of 1 min. The cooling rate in all cases was 10 K/s.

High-resolution EBSD mappings were performed in the longitudinal section of both samples in order to investigate its recrystallization behavior. The microstructure of the annealed specimens was imaged using a JEOL-6500F field emission gun scanning electron microscope (FEG-SEM) operated at 15 kV. Texture data at the grain scale were obtained by automated acquisition and further indexing of Kikuchi patterns after image processing in a TSL system interfaced to the SEM. Vickers microhardness testing was performed in longitudinal sections of the specimens using a load of 200 g. Following, TEM samples were obtained from this material by applying electropolishing at a potential of 12 V using an 80% methanol–20% H_2SO_4 solution (in vol.%) at 20 °C and precise ion polishing at both sides. TEM investigation was performed on the rolling plane (RD–TD plane, where RD and TD are the rolling direction and the transverse direction, respectively) using Philips CM30 (300 kV) and FEI TECNAI-20F microscopes.

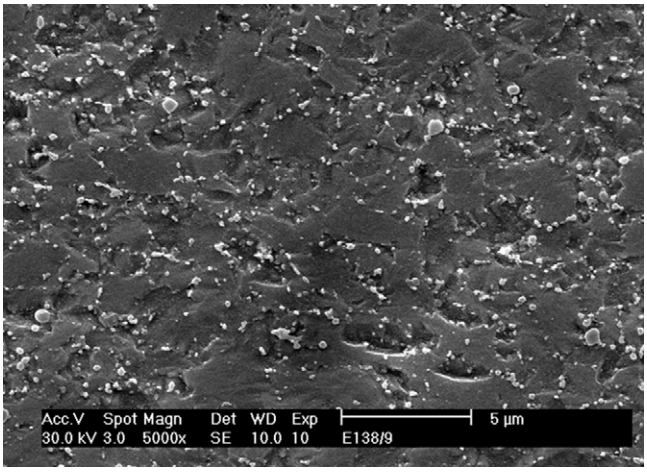

Fig. 1. Microstructure of the reduced activation ferritic–martensitic 9% Cr–ODS–Eurofer steel in the as-received condition (SEM, secondary electrons image). The rolling direction (RD) is parallel to the scale bar.

3. Results and discussion

3.1. Initial microstructure

The microstructure of this steel in the as-received condition (quenched and tempered martensite at 750 °C for 2 h) consists of grains with a mean size of about 3 μm (Fig. 1). They are slightly elongated as the hot rolling process did not lead to complete recrystallization of the sheets. Both nanoscale Y_2O_3 and coarse $M_{23}C_6$ particles are found in the ferritic Fe–Cr matrix. Their respective volume fractions are about 0.5% and 1.5%. A detailed description of the microstructure of this steel in terms of particle sizes and their distributions are found elsewhere [15,16].

3.2. Softening behavior

The softening behavior of the steel is shown in Fig. 2. Two distinct rolling reductions (50% and 80%) were chosen for comparison. The data reveal that the amount of softening experienced by this steel is quite small even after annealing at 800 °C for 1 h. The respective values of the calculated amount of softening are 3% and 7% for 50% and 80% reductions. This clearly means that recrystallization is not pronounced in this steel even after such large straining. In

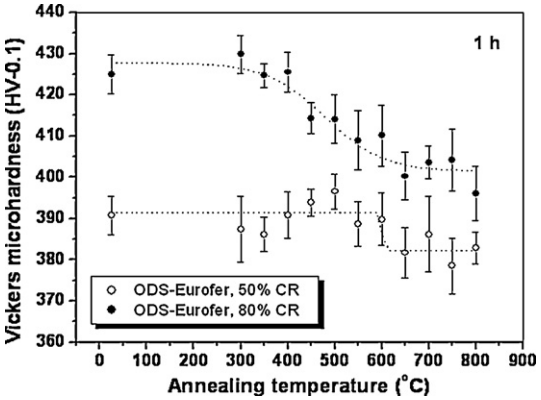

Fig. 2. Softening behavior of the reduced activation ferritic–martensitic 9%Cr–ODS–Eurofer steel after 50% and 80% reductions.

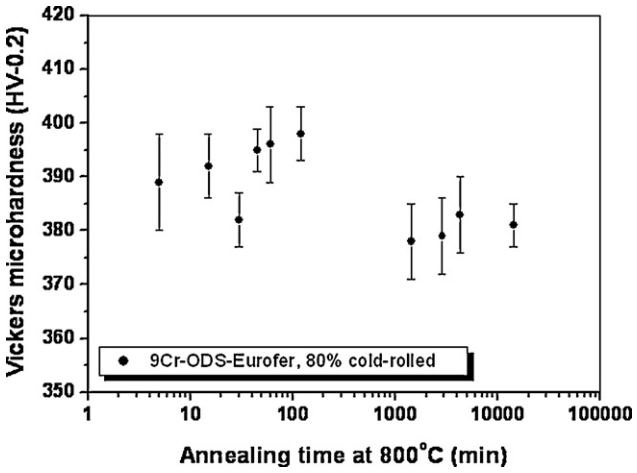

Fig. 3. Softening kinetics of the RAFM–9%Cr–ODS–Eurofer steel at 800 °C after 80% cold rolling.

order to follow its behavior for longer isothermal annealing periods, the corresponding softening kinetics curve was determined for the 80% cold rolled steel annealed at 800 °C (see Fig. 3). Results show that the hardness remains nearly unchanged even after isothermal annealing for 10 days at this temperature indicating that this steel has a high thermal stability. The maximum annealing temperature was set at 800 °C to ensure that annealing was performed in the ferritic phase field. The limit temperature for the ferritic phase field was confirmed by high-temperature dilatometry tests and Table 1 shows the values of A_{c1}, A_{c3} and M_s found for three different heating rates.

3.3. EBSD investigation

The EBSD scans were carried out in longitudinal sections of representative samples in two conditions: 50% and 80% cold rolling both followed by annealing at 800 °C for 1 h (Fig. 4a and b, respectively). EBSD sampling points were taken in 50 nm steps. The EBSD scans revealed important details of the annealed structure of the ODS–Eurofer steel. Elongated grains along the rolling direction are found throughout the microstructure in the sample rolled to 80%.

Table 1
A_{c1}, A_{c3} and M_s temperatures determined by dilatometric tests in the RAFM–9%Cr–ODS–Eurofer steel.

Heating rate (K/s)	A_{c1} (°C)	A_{c3} (°C)	M_s (°C)
1	835	915	345
5	850	940	350
30	875	985	360

Coarser features are noticed in the less deformed specimen, i.e. grains are less flattened than at 80% reduction. The analysis of the corresponding microtexture data from EBSD scans reveals orientations that mostly belong to the α- and γ-fibers [8]. The α-fiber texture component has a ⟨1 1 0⟩ fiber axis parallel to the rolling direction (RD) of the rolled sheet. The γ-fiber has a fiber axis ⟨1 1 1⟩ perpendicular to the sheet surface. These orientation fibers are found in bcc metals and alloys and they can be easily visualized at the corresponding orientation distribution function (ODF) sections with $\varphi_2 = 0°$ and $\varphi_2 = 45°$ (Bunge notation). An overview of the textures in such ferritic stainless steels is given in Ref. [17].

The ODFs corresponding to the samples deformed to 50% and 80% and annealed at 800 °C for 1 h are shown in Fig. 5. The texture components found in these samples are typical of low-carbon steels (α- and γ-fibers at $\varphi_2 = 45°$, rotated cube at $\varphi_2 = 0°$) [18]. The large orientation spread around the rotated cube orientation in the 50% rolled material may be caused by local effects. For 50% reduction, the γ-fiber appears more intense than the α-fiber. For 80% reduction, the α-fiber is strengthened with a maximum close to {1 1 2}⟨1 1 0⟩–{1 1 3}⟨1 1 0⟩ while γ-fiber is slightly weakened with a maximum close to {1 1 1}⟨1 1 0⟩. The strength of the γ-fiber in low-carbon steels depends on the applied strain. Hutchinson reported that it increases up to 70% and the remains nearly constant for larger strains [19]. The results shown in Fig. 5 are similar to those reported in the literature for the deformation texture of cold rolled low-carbon and Fe–Cr steels [19,20]. They match quite reasonably texture data obtained from XRD within statistical limits. The low recrystallized volume fraction found in the annealed samples does not change significantly the texture. Recovery does not change the texture so that these samples retain most of the rolling texture components.

In the EBSD scans it is also possible to notice the presence of a low volume fraction of tiny equiaxed grains at the prior grain

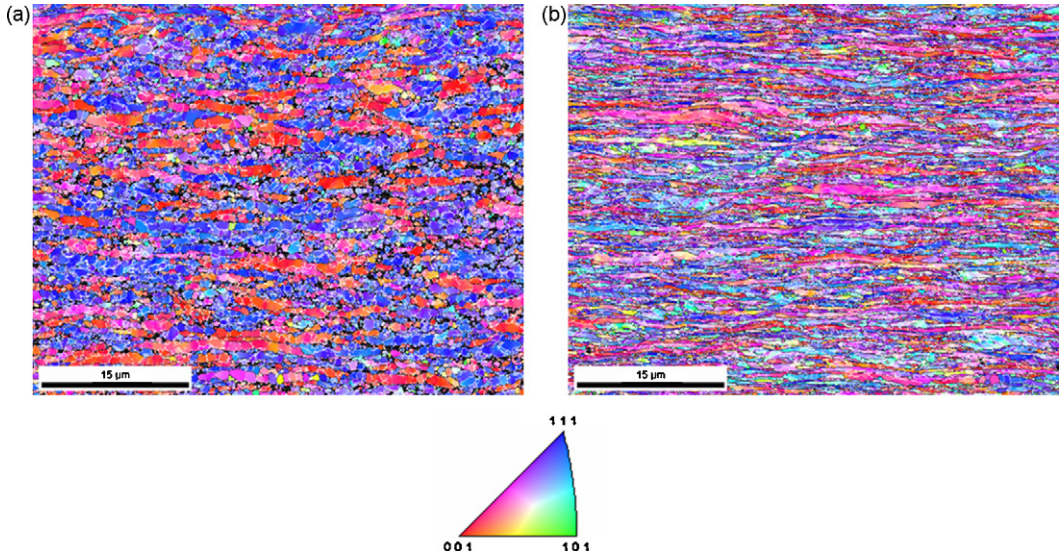

Fig. 4. High-resolution EBSD scans in longitudinal sections of RAFM–9%Cr–ODS–Eruofer steel: (a) 50% reduction + annealing at 800 °C for 1 h. (b) 80% reduction + annealing at 800 °C for 1 h. High angle boundaries (above 15°) are marked by black lines while low angle boundaries (2–15°) are marked by white lines (step size: 50 nm). The rolling direction (RD) is parallel to the scale bar.

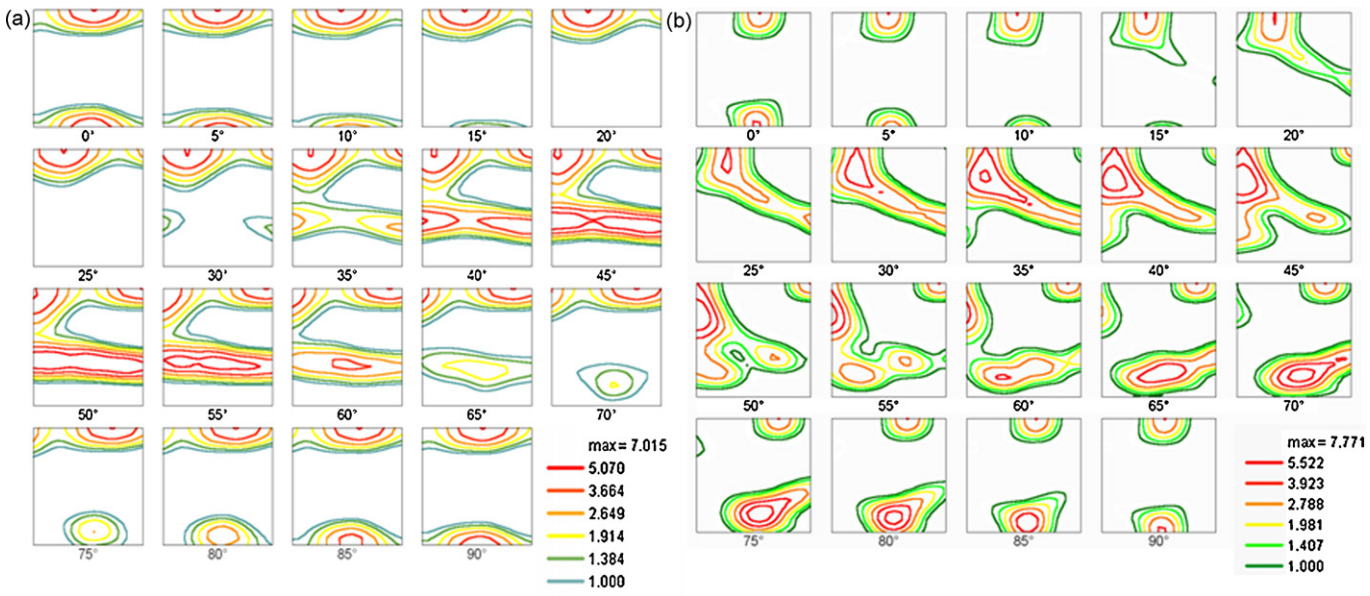

Fig. 5. Orientation distribution function (ODF) plots of RAFM–9%Cr–ODS–Eurofer corresponding to the EBSD scans shown in Fig. 4: (a) 50% reduction + annealing at 800 °C for 1 h; (b) 80% reduction + annealing at 800 °C for 1 h.

boundaries. These small grains result from static recrystallization during annealing at 800 °C. The new recrystallized grains can be distinguished from the recovered matrix in the EBSD scans because they are most equiaxed whereas the prior grains are larger, elongated in shape and subdivided by low angle boundaries. The microstructures depicted in Fig. 4 are rather similar to those found in low-carbon steels (recovered state) with elongated grains belonging to both α- and γ-fiber texture components [8,19]. A closer inspection at the EBSD scans reveals the occurrence of important orientation effects regarding grain subdivision in this steel. Fig. 6a shows an enlarged view of a sample deformed to 80% reduction and annealed at 800 °C for 1 h. Misorientation profiles were taken at two distinct grains: grain A (α-fiber) and grain B (γ-fiber) and the results are shown respectively,

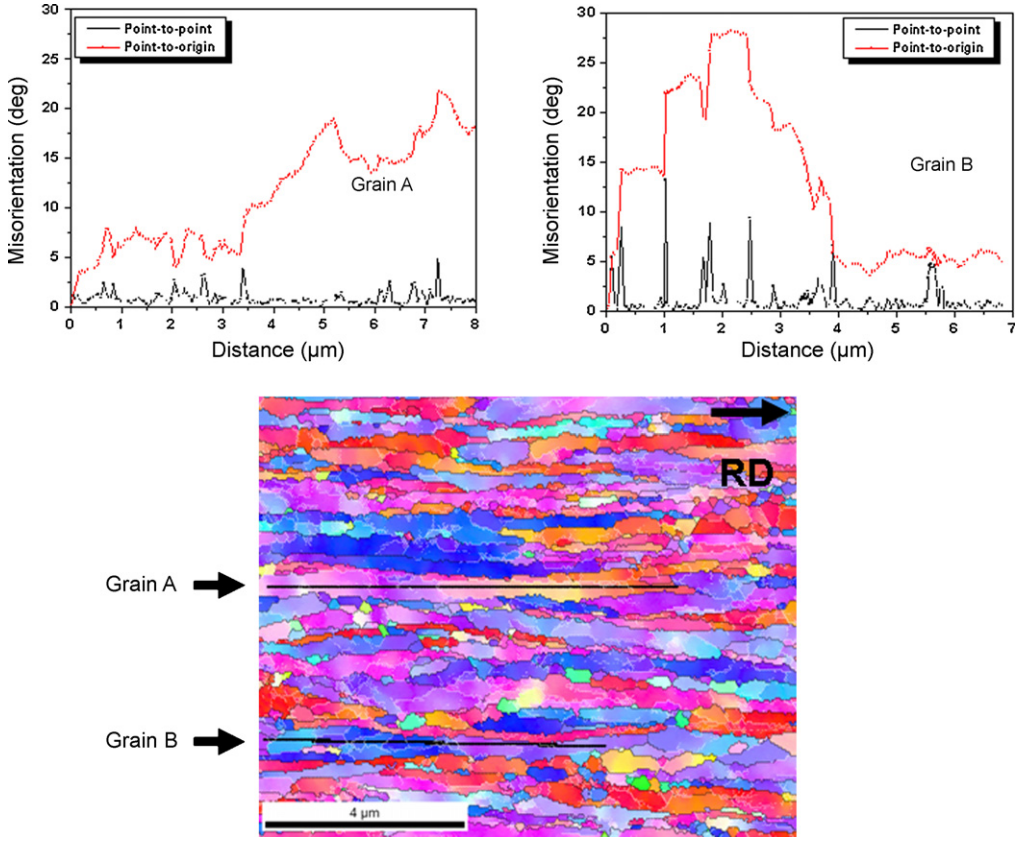

Fig. 6. Misorientation profiles taken in grains A and B showing distinct fragmentation in the RAFM–9%Cr–ODS–Eurofer steel deformed to 80% and annealed at 800 °C for 1 h. HABs (above 15°) are marked in black and LABs (2–15°) in white. The rolling direction (RD) is parallel to the scale bar.

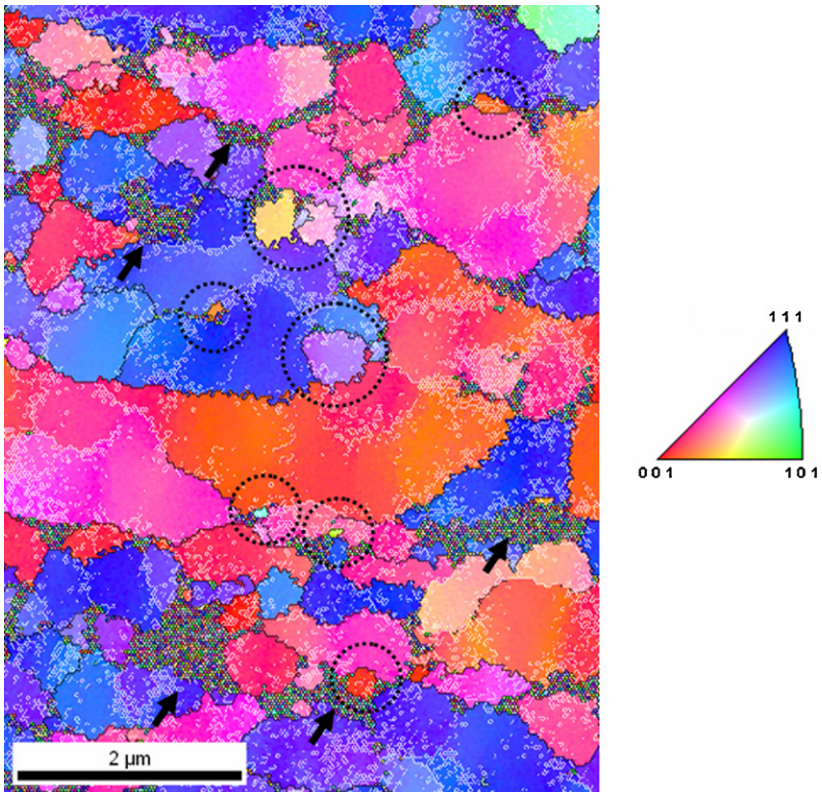

Fig. 7. Orientation map showing small angle (2–15°, white lines) and high angle boundaries (above 15°, black lines) in the RAFM–9%Cr–ODS–Eurofer steel deformed to 50% and annealed at 800 °C for 1 h (step size of 30 nm). Coarse $M_{23}C_6$ particles were not indexed and are indicated by arrows. The rolling direction (RD) is parallel to the scale bar.

in Fig. 6b and c. Point-to-point and point-to-origin misorientations are plotted for both grains. Notice that grain A has much smaller in-grain orientation gradients than grain B. The misorientations found in grain A are within the range 2–4° whereas in grain B this value commonly reaches 10–14°. These features are frequently observed throughout the microstructure. Grains belonging to the α-fiber are less fragmented than grains with individual orientations belonging to the γ-fiber [21]. Misorientation profiles taken across many cells/subgrains in annealed samples confirm this trend. This finding is very important because it affects the amount of stored energy for recrystallization, i.e., the more fragmented a grain is, the higher is its stored energy. Also the occurrence of highly curved zones in as-deformed grains is an essential pre-requisite for the formation of recrystallization nuclei.

Thus, our results also confirm that γ-fiber oriented grains are more prone to undergo recrystallization than α-fiber grains. These findings are in agreement with those reported in the literature for iron and conventional low-carbon steels using several characterization techniques [22–24].

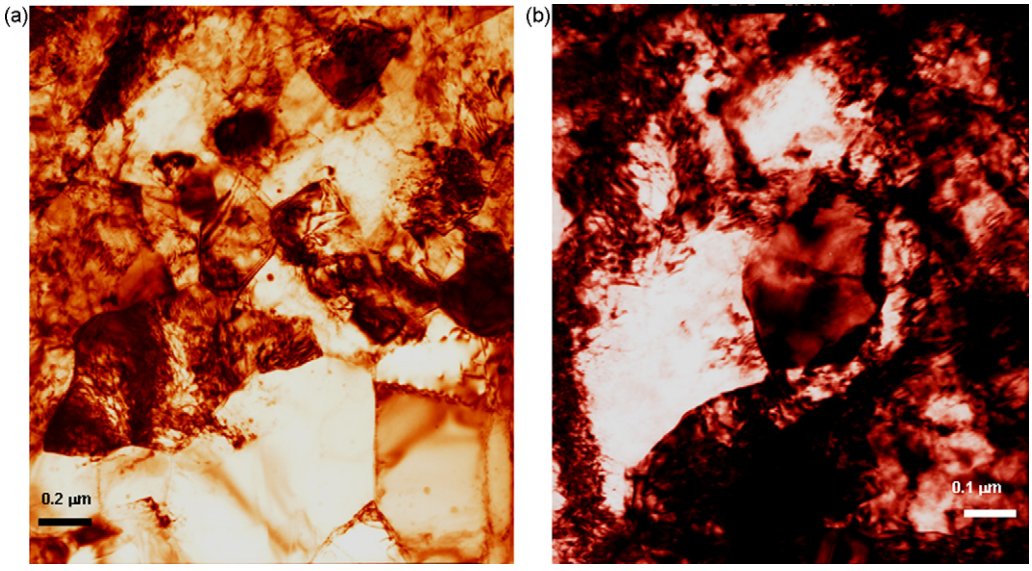

Fig. 8. TEM bright field images of a sample deformed to 80% and annealed at 800 °C for 1 h showing: (a) $M_{23}C_6$ carbide particles, recrystallized, and recovered grains in close vicinity; (b) enlarged view of a large carbide particle and a recrystallization nucleus around it in detail (PSN). The rolling direction (RD) is parallel to the scale bar.

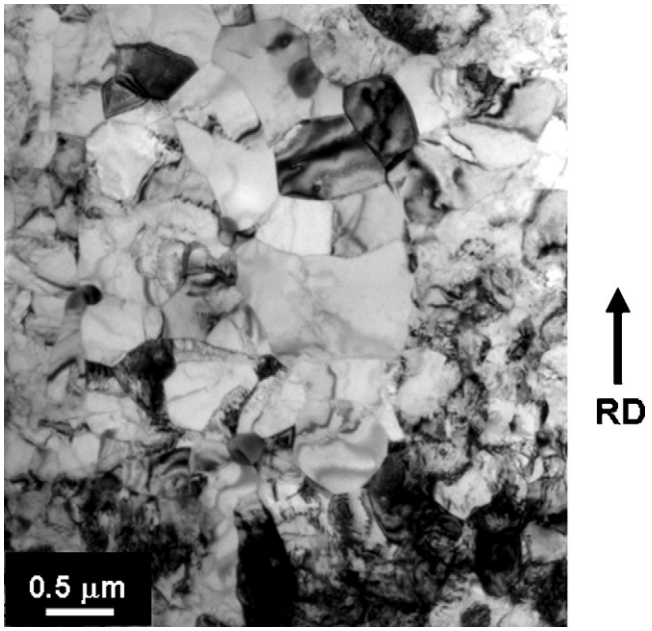

Fig. 9. TEM bright field micrograph showing the general view of the microstructure of the steel deformed to 80% and annealed at 800 °C for 48 h. Recrystallized grains (center) and recovered regions are noticeable.

Another important result depicted in Fig. 6a reveals where the recrystallization nuclei are found. They typically occur at prior grain boundaries, either at α–α, α–γ or γ–γ grain boundaries. This nomenclature refers to the orientation fiber to which each grain belongs (α- or γ-fibers). In most cases, the recrystallization front tends to migrate towards the interior of γ-fiber oriented grains because of their higher stored energy. Only in a very few cases, nucleation in the interior of the grains is observed and when it occurs, it is associated with the presence of lamellar boundaries. In all cases, the new grains do not grow very much and remain in a size range of 0.2–1 μm. The assumptions to explain why they do not grow are discussed later when the TEM results are presented and discussed.

We have also performed an additional EBSD mapping with a finer step size of 30 nm in the less deformed specimen (50% + annealing at 800 °C for 1 h), as shown in Fig. 7. In this figure it is possible to identify recrystallized grains (marked by circles) and nearly equiaxed cell structures (or subgrains) with misorientations above 2° subdividing the grains. Boundaries with misorientations below 2° cannot be properly indexed by EBSD. In this case, TEM provides a better resolution of the misorientation across these boundaries. This microstructure is typical of recovered or partially recrystallized metals. It is worth mentioning that there are regions where indexing of Kikuchi patterns was not possible like those corresponding to coarse $M_{23}C_6$ particles, pores, or deformed areas at grain boundaries (higher dislocation density). Jagged high angle grain boundaries (marked with black lines) are also noticeable as a result of particle–boundary interaction (Zener pinning).

3.4. TEM investigation

The microstructures of annealed samples were observed in TEM to resolve details of the particle–boundary interaction and to determine the preferential nucleation sites for recrystallization. As a general remark, recovered structures (diffuse dislocation tangles and low angle boundaries) as well as free dislocations are the predominant microstructural features in the annealed samples. Recrystallized grains are mostly observed at the prior grain boundaries and around coarse carbide particles. These findings are in agreement with those obtained from high-resolution EBSD mappings.

Fig. 8 shows the typical microstructure of a sample deformed to 80% reduction and annealed at 800 °C for 1 h. Fig. 8a shows the general view of the microstructure. Particles, subgrains and a few recrystallized areas (lower part of the micrograph) can be noticed. Fig. 8b, on the other hand, shows an enlarged view of a neighboring area where a recrystallized grain formed around a coarse $M_{23}C_6$ particle can be seen, another evidence of particle stimulated nucleation in this material. It is worth mentioning that only a minor portion of the recrystallized grains can be explained by PSN mechanism in ODS–Eurofer steel. Further TEM investigation is necessary to obtain more quantitative data.

Even for longer annealing times at 800 °C (48 h, for instance), the microstructure did not change too much (Fig. 9). The micrograph shows a cluster of recrystallized grains surrounded by a recovered matrix. The volume fraction of recrystallized grains remains below 10%. The fine dispersion of Y-based particles cannot be properly resolved at this low magnification. Fig. 10a shows a typical Y-based particle (high-resolution TEM). The former Y_2O_3 particles added to the metallic powder for high energy milling may react with chromium during high-temperature hot-isostatic con-

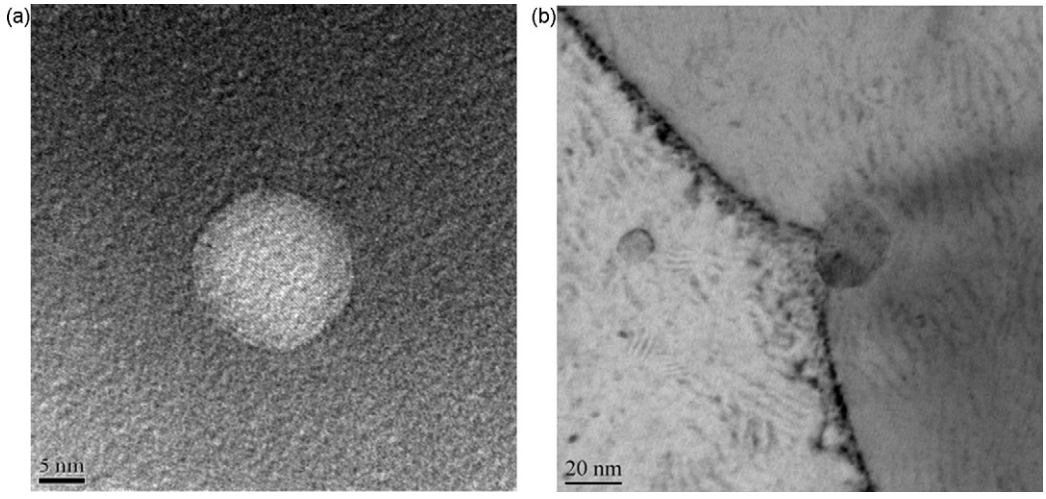

Fig. 10. High-resolution transmission electron micrographs of a sample deformed to 80% and annealed at 800 °C for 48 h showing: (a) individual $YCrO_3$ particle in the ferritic matrix; (b) dragging effect (particle–boundary interaction) during annealing. The rolling direction (RD) is parallel to the scale bar.

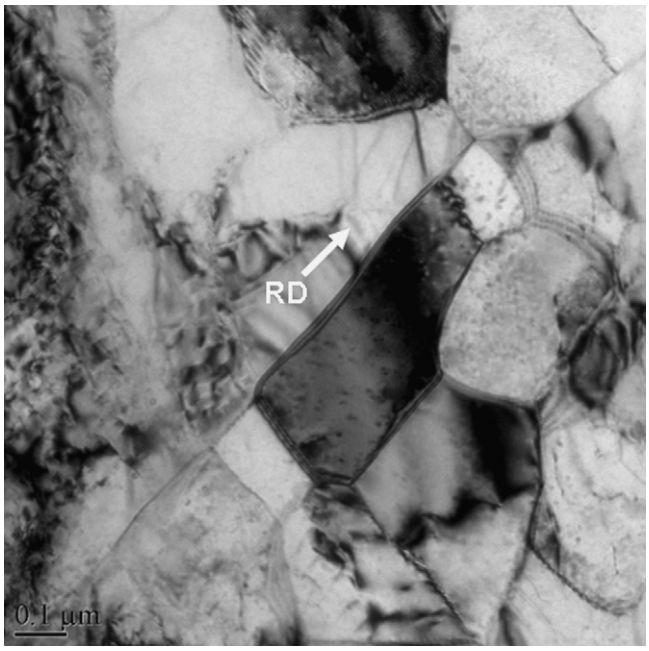

Fig. 11. TEM bright field micrograph showing nucleation of recrystallized grains at prior grain boundaries in a sample deformed to 80% and annealed at 800 °C for 1 h.

solidation forming, for instance, $YCrO_3$ particles [25]. It is worth mentioning that this compound is already present in the steel in the as-received condition.

Fig. 10b provides a good example of the retarding effect found during particle–boundary interaction in this steel. The rearrangement of dislocations and the thermally-assisted migration of low and high angle boundaries during annealing become difficult since they are pinned or retarded by particles making recrystallization very sluggish. In our view, the presence of tiny recrystallized grains in the annealed state can be explained by the following nucleation mechanisms:

(a) Highly deformed regions evolve around coarse particles during cold rolling. Upon annealing, subgrain growth takes place and the misorientations around particles may reach high angle character (above 15°). The local stored energy is large enough to sustain its growth until reaching a critical size (smaller than 1 μm). Due to competing recovery reactions, the driving force decreases continuously and recrystallization stops.
(b) High angle boundaries are also present in the deformed state, especially after such a large straining. Prior grain boundaries and deformation-induced lamellar boundaries (see Fig. 11) can be noticed in the microstructure and provide the necessary mobile interface to trigger recrystallization. The stored energy at prior grain boundaries is larger than the one found in the interior of the grains which helps to sustain the growth of the recrystallization nuclei.

The explanation for why static recrystallization is almost suppressed in this steel can be summarized as follows:

Nucleation takes place in deformation zones around coarse $M_{23}C_6$ carbide particles and at the grain boundaries. The combination of retarding effects such as Zener pinning and competing recovery decrease the local stored energy and impede further growth of the recrystallization nuclei. These results confirm the expected high thermal stability of this steel, at least when annealing is performed in the ferritic phase field (below 800 °C).

4. Conclusions

(1) It has been shown that static recovery is the main softening mechanism in 9%Cr–ODS–Eurofer steel when annealed in the ferritic regime (below 800 °C).
(2) Complete static recrystallization is prevented due to the strong interaction between boundaries and the fine dispersion of stable Y_2O_3 particles even after severe cold rolling to 80% reduction and annealing at 800 °C for long periods (240 h). The recrystallized volume fraction is very small (below 0.10) and the few recrystallization nuclei were found predominantly clustered at prior grain boundaries and around large $M_{23}C_6$ carbide particles.
(3) It has also been observed that nucleation for recrystallization occurs preferentially in grains whose orientation belongs to the γ-fiber texture component. When nucleation occurs at grain boundary regions, the recrystallization front tends to migrate towards the interior of γ-fiber grains due to their higher stored energy.

Acknowledgments

The authors would like to acknowledge the support provided by FAPESP (Grants 07/56.436-0 and 08/54.064-1) and CNPq (Grant 484.355/2007-4) for the development of this work. HRZS is also indebted to Katja Angenendt (MPI-E) for her kind assistance in high-resolution EBSD measurements.

References

[1] K. Ehrlich, W. Cierjacks, S. Kelzenberg, A. Moeslang, in: D. Gelles et al. (Eds.), 17th International Symposium on Effects of Radiation on Materials, ASTM STP 1270, 1996, pp. 1109–1122.
[2] M.R. Gilbert, R.A. Forrest, Handbook of Activation Data Calculated Using EASY-2003, Report UKAEA FUS 509, July 2004.
[3] S. Jitsukawa, M. Tamura, B. van der Schaaf, R.L. Klueh, A. Alamo, C. Petersen, M. Schirra, P. Spaetig, G.R. Odette, A.A. Tavassoli, K. Shiba, A. Kohyama, A. Kimura, J. Nucl. Mater. 307–311 (2002) 179–186.
[4] R. Lindau, A. Möslang, M. Schirra, Fusion Eng. Des. 61–62 (2002) 659–664.
[5] B. van der Schaaf, F. Tavassoli, C. Fazio, E. Rigal, E. Diegele, R. Lindau, G. Le Marois, Fusion Eng. Des. 69 (2003) 197–203.
[6] R. Lindau, A. Möslang, M. Rieth, Fusion Eng. Des. 75–79 (2005) 989–996.
[7] A. Möslang, Ch. Adelhelm, R. Heidinger, Int. J. Mater. Res. 99 (2008) 1045–1054.
[8] F.J. Humphreys, M. Hatherly, Recrystallization and Related Annealing Phenomena, Pergamon, 1996.
[9] J. Konrad, S. Zaefferer, D. Raabe, Acta Mater. 54 (2006) 1369–1380.
[10] F.J. Humphreys, M.G. Ardakani, Acta Mater. 44 (1996) 2711–2716.
[11] A.O.F. Hayama, H.R.Z. Sandim, J.F.C. Lins, M.F. Hupalo, A.F. Padilha, Mater. Sci. Eng. A 371 (2004) 198–209.
[12] M. Klimiankou, R. Lindau, A. Möslang, J. Nucl. Mater. 367–370 (2007) 173–178.
[13] K. Maruyama, K. Sawada, J. Koike, ISIJ Int. 41 (2001) 641–653.
[14] J. Pešička, R. Kužel, A. Dronhofer, G. Eggeler, Acta Mater. 51 (2003) 4847–4862.
[15] R. Schaeublin, T. Leguey, P. Spätig, N. Baluc, M. Victoria, J. Nucl. Mater. 307–311 (2002) 778–782.
[16] M. Klimiankou, R. Lindau, A. Moslang, J. Nucl. Mater. 329–333 (2004) 347–351.
[17] M. Hölscher, D. Raabe, K. Lücke, Steel Res. 62 (1991) 567–575.
[18] D. Raabe, Steel Res. Int. 74 (2003) 327–337.
[19] B. Hutchinson, Phil. Trans. R. Soc. Lond. A 357 (1999) 1471–1485.
[20] D. Raabe, K. Lücke, Mater. Sci. Technol. 9 (1993) 302–312.
[21] D. Raabe, Steel Res. 66 (1995) 222–229.
[22] I.L. Dillamore, C.J.E. Smith, T.W. Watson, Met. Sci. J. 1 (1967) 49–54.
[23] I. Samajdar, B. Verlinden, P. Van Houtte, D. Vanderschueren, Mater. Sci. Eng. A 238 (1997) 343–350.
[24] A. Borbély, J.H. Driver, T. Ungár, Acta Mater. 48 (2000) 2005–2016.
[25] M. Klimiankou, R. Lindau, A. Möslang, J. Cryst. Growth 249 (1–2) (2003) 381–387.